



Pterostilbene fluorescent probes as potential tools for targeting neurodegeneration in biological applications

Lidia Ciccone, Susanna Nencetti, Maria Marino, Chiara Battocchio, Giovanna Iucci, Iole Venditti, Martina Marsotto, Emiliano Montalesi, Simone Socci, Beatrice Bargagna & Elisabetta Orlandini

To cite this article: Lidia Ciccone, Susanna Nencetti, Maria Marino, Chiara Battocchio, Giovanna Iucci, Iole Venditti, Martina Marsotto, Emiliano Montalesi, Simone Socci, Beatrice Bargagna & Elisabetta Orlandini (2022) Pterostilbene fluorescent probes as potential tools for targeting neurodegeneration in biological applications, Journal of Enzyme Inhibition and Medicinal Chemistry, 37:1, 1812-1820, DOI: [10.1080/14756366.2022.2091556](https://doi.org/10.1080/14756366.2022.2091556)

To link to this article: <https://doi.org/10.1080/14756366.2022.2091556>



© 2022 The Author(s). Published by Informa UK Limited, trading as Taylor & Francis Group.



[View supplementary material](#)



Published online: 27 Jun 2022.



[Submit your article to this journal](#)



Article views: 493



[View related articles](#)



[View Crossmark data](#)

BRIEF REPORT



Pterostilbene fluorescent probes as potential tools for targeting neurodegeneration in biological applications

Lidia Ciccone^{a,b} , Susanna Nencetti^{a,b}, Maria Marino^c, Chiara Battocchio^c, Giovanna Iucci^c, Iole Venditti^c, Martina Marsotto^c, Emiliano Montalesi^c, Simone Socci^d, Beatrice Bargagna^d and Elisabetta Orlandini^{d,e}

^aDepartment of Pharmacy, University of Pisa, Pisa, Italy; ^bCISUP – Centre for Instrumentation Sharing, University of Pisa, Pisa, Italy; ^cDepartment of Science, University Roma Tre, Rome, Italy; ^dDepartment of Earth Science, University of Pisa, Pisa, Italy; ^eResearch Centre E. Piaggio, University of Pisa, Pisa, Italy

ABSTRACT

Several epidemiological studies suggest that a diet rich in fruit and vegetables reduces the incidence of neurodegenerative diseases. Resveratrol (Res) and its dimethylated metabolite, pterostilbene (Ptb), have been largely studied for their neuroprotective action. The clinical use of Res is limited because of its rapid metabolism and its poor bioavailability. Ptb with two methoxy groups and one hydroxyl group has a good membrane permeability, metabolic stability and higher *in vivo* bioavailability in comparison with Res. The metabolism and pharmacokinetics of Ptb are still sparse, probably due to the lack of tools that allow following the Ptb destiny both in living cells and *in vivo*. In this contest, we propose two Ptb fluorescent derivatives where Ptb has been functionalised by benzofurazan and rhodamine-B-isothiocyanate, compounds **1** and **2**, respectively. Here, we report the synthesis, the optical and structural characterisation of **1** and **2**, and, their putative cytotoxicity in two different cell lines.

ARTICLE HISTORY

Received 13 April 2022
Revised 7 June 2022
Accepted 13 June 2022

KEYWORDS

Ptb fluorescent probes; spectrophotometric; pterostilbene 7-nitrobenzofurazan (NBD) derivative; pterostilbene rhodamine-B-isothiocyanate (Rh B-Itc) derivative; cytotoxicity

1. Introduction

Neurodegenerative diseases such as Parkinson's (PD), Alzheimer's AD, Amyotrophic Lateral Sclerosis (ALS), and Macular Degeneration (MS) are considered the greatest challenge for all researchers in the twenty-first century. It has been hypothesised that, in 2030, the incidence of only AD, in the world population, will be around 100 million individuals, with a very high emotional and economic cost^{1,2}.

Unfortunately, the treatments available against these pathologies are not effective and, in most cases cannot prevent the onset of the disease^{3–6}. Only in some cases, they allow the slowing of pathology progression guaranteeing, for short periods, an acceptable quality of life. On 7 June 2021, the Food and Drug Administration (FDA) approved Aduhelm (aducanumab) a human IgG1 anti-A β monoclonal antibody specific for β -amyloid oligomers and fibrils for the treatment of AD⁷, although, the scientific community has still conflicting opinions^{8,9}.

Therefore, it appears very important to focus the attention on the research to prevent or to slow down the initial steps of the neurodegeneration process. The discovery of promising agents against neurodegeneration with little or no toxicity represents an important goal for all people suffering from this debilitating disease and their caregivers.





Recently, several studies have confirmed that plant derived natural substances, whether of terrestrial or marine origin can reduce the incidence of different pathologies including neurodegenerative^{10–14}, cancer and heart diseases^{15,16}, chronic


inflammation and arthritis^{17,18}. Among several promising compounds, resveratrol (Res) is one of the most studied and best known for its potential as a therapeutic agent for neurodegenerative diseases^{19–21}. Res is a polyphenol (trans-3,4,5-trihydroxystilbene), **Figure 1**, found in several plants, grapes, blueberries raspberries and peanuts. Several *in vitro* and *in vivo* studies^{22–25} report that Res is a promising compound for the prevention and the treatment of the neurodegeneration. In particular, in a randomised double-blind placebo-controlled trial versus AD reported that Res is well-tolerated and safe for the patients²⁶.

However, the clinical use of Res is limited because of its rapid metabolism and its poor bioavailability, encouraging researchers to derivatize this stilbene to overcome its limit²⁷. In parallel, new polyphenols were studied for their neuroprotective effects. In particular, the researches have turned attention on the polyphenol pterostilbene (Ptb) (trans 4-(3,5-dimethoxystyryl)phenol); the dimethyl analogue of Res (**Figure 1**) found among other foods, in grapes, blueberries and almonds^{28,29}.

Studies show that, following oral administration, Ptb has an approximately 4-fold greater (about 80% versus 20%) bioavailability and 7.5-fold (105 min versus 14 min) longer half-life if compared to Res^{30,31}. As a whole, compared with Res, Ptb seems to have a better membrane permeability and metabolic stability, which subsequently could increase its bioavailability and pharmacokinetic profile³².

Recent studies have demonstrated that Ptb has anti-inflammatory, anti-carcinogenic and anti-diabetic and neuroprotective

CONTACT Elisabetta Orlandini  elisabetta.orlandini@unipi.it  Department of Earth Science, University of Pisa, Via Santa Maria, 53, 56126 Pisa, Italy; Susanna Nencetti  susanna.nencetti@unipi.it  Department of Pharmacy, University of Pisa, Via Bonanno 6, 56126 Pisa, Italy

 Supplemental data for this article is available online at <https://doi.org/10.1080/14756366.2022.2091556>

© 2022 The Author(s). Published by Informa UK Limited, trading as Taylor & Francis Group.

This is an Open Access article distributed under the terms of the Creative Commons Attribution License (<http://creativecommons.org/licenses/by/4.0/>), which permits unrestricted use, distribution, and reproduction in any medium, provided the original work is properly cited.

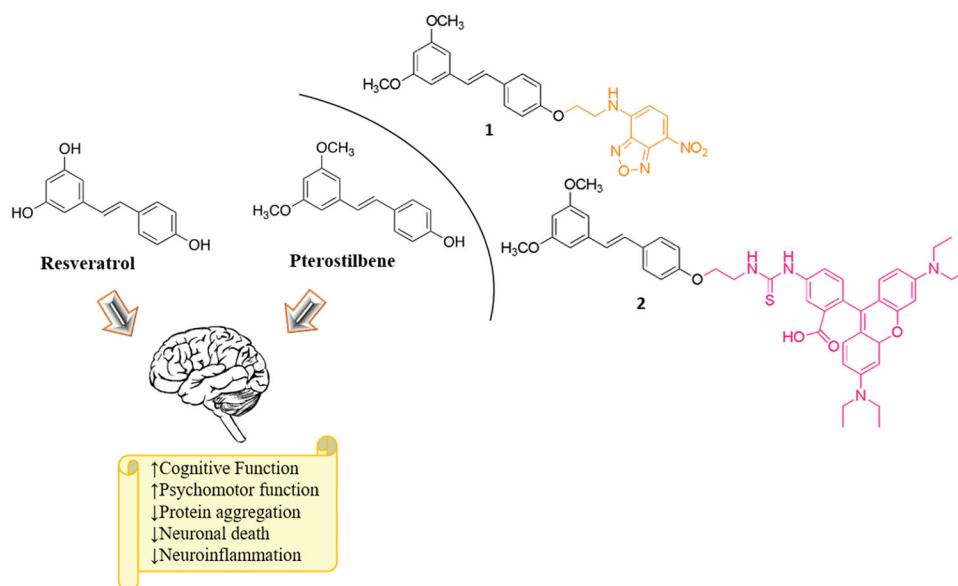


Figure 1. Chemical structures of resveratrol (Res) and pterostilbene (Ptb) and their positive effects in the brain. On the right side the structure of Ptb functionalised on phenolic ring with benzofurazan **1** (yellow) and with rhodamine B-isothiocyanate **2** (pink), respectively.

properties together with a very low toxicity in animal and human models^{29,33–38}. The low molecular weight and good liposolubility allow Ptb to pass through the blood–brain barrier improving neurological function after ischaemia reperfusion, exerting a neuroprotective effect³⁹. Moreover, Ptb mediates neuroprotective activity mainly *via* the subtype α of oestrogen receptor (ER- α) and may be a new neuroprotective agent for nerve injury treatment and prevention⁴⁰.

However, the metabolism and pharmacokinetics of Ptb are still scarce probably due to the lack of tools that allow following the Ptb destiny both in living cells and *in vivo*³².

Here, new fluorescent derivatives of Ptb **1** and **2** (Figure 1) have been synthesised and characterised to highlight their fluorescent properties *in vitro* and to evaluate their putative cytotoxicity in two different cell lines. Compound **1** possesses benzofurazan (2,1,3-benzoxadiazole, NBD) as fluorescent moiety while compound **2** is functionalised with rhodamine-B-isothiocyanate (Rhd B-Itc) (Figure 1). The use of fluorescent probes could be useful in the evaluation of the molecular pathways involved in neuroprotection process.

2. Result and discussion

2.1. Chemistry experimental procedures

Compounds **1** and **2** were synthesised as reported in Scheme 1, following the synthetic route reported in the literature for Res fluorescent compounds⁴¹.

In detail, compounds **1** and **2** were synthesised *via* amine derivative **6** that was obtained from the reaction of Ptb with *N*-Boc-bromoethylamine, and subsequent deprotection of the Boc group in acidic conditions. After, the conjugation of compound **6** with benzofurazan (2,1,3-benzoxadiazole, NBD) or rhodamine-B-isothiocyanate (Rhd B-Itc) afforded the desired fluorescent pterostilbene derivatives **1** and **2**.

For compound **1**, the NBD was chosen as fluorescent probe skeleton because the NBD fluorescent derivatives possess long excitation and emission wavelengths (e.g. 464 nm, em. 512 nm) that avoid interference due to biomatrices as reported in the literature^{42,43}. While, compound **2** was functionalised with Rhd B-Itc;

a moiety present in numerous fluorescent compounds used to perform biological tests⁴⁴.

2.2. Optical and structural characterizations

UV–visible absorption and emission characterisations were carried out on NBD, Res, **1** and **2** compounds. For all samples, absorption spectra were collected in DMSO solutions prepared at three different concentrations, and the respective calibration lines were obtained by applying a linear fitting procedure (origin included), as to calculate the molar extinction coefficient (ϵ). Maximum absorption wavelengths and ϵ values are summarised in Table 1.

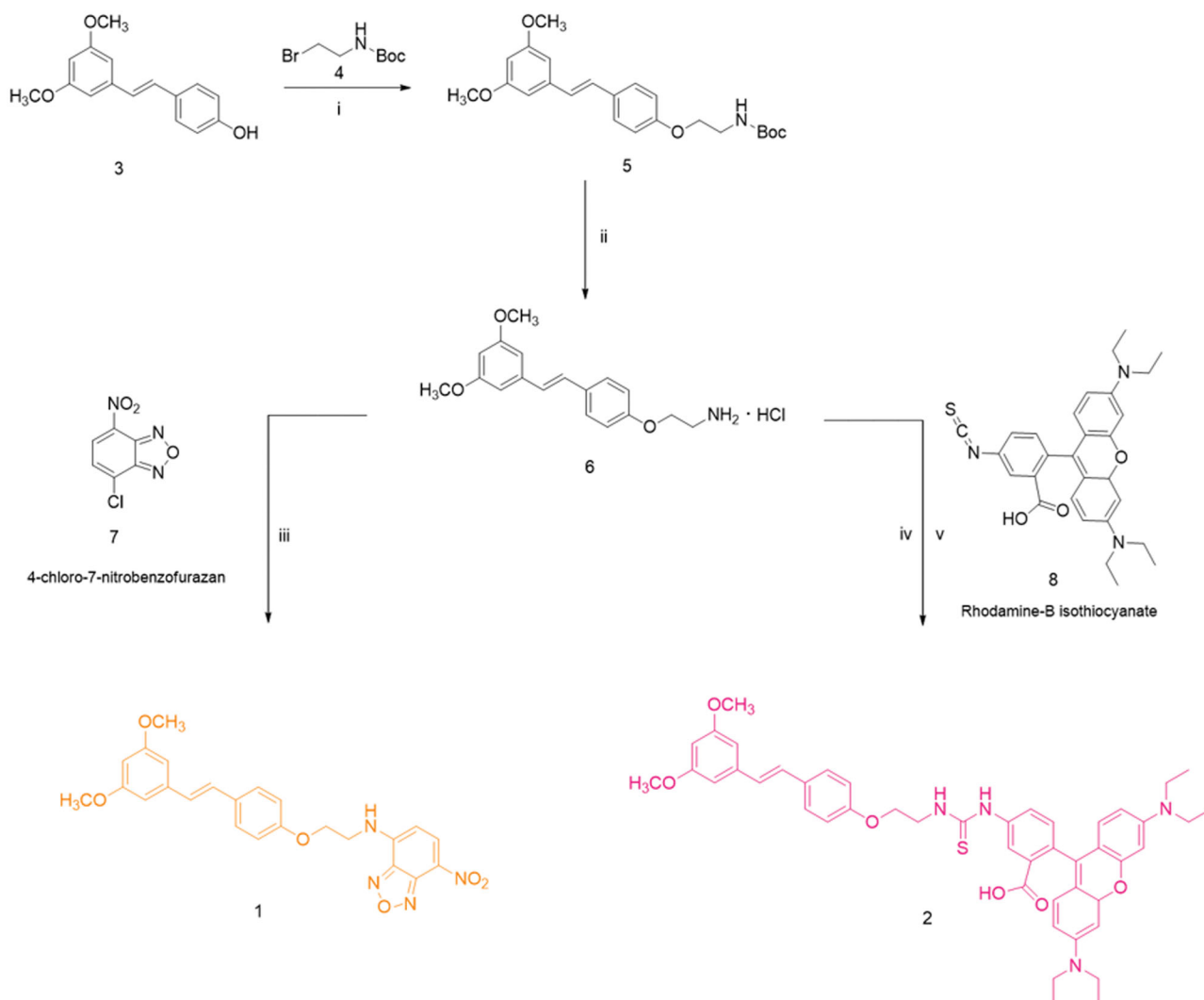
Emission spectra were also collected by exciting the four samples DMSO solutions at the maximum absorption wavelength. Excitation wavelength (λ_{exc}), emission wavelength (λ_{emis}), and emission intensity (I_{emis}) values are summarised in Table 2. All absorption and emission spectra and linear fits are reported in the Supporting material (Figures S1–S5), as well as absorption wavelengths, absorbance values, emission wavelengths, and emission intensity values for each measured solution (Tables S1–S5).

The absorption and emission spectra collected on **1** and **2** are shown in Figure 2.

The proposed molecular structure of samples **1** and **2** was also assessed in solid state by Near-Edge X-ray Absorption Fine Structure spectroscopy (NEXAFS). NEXAFS spectra are reported in Figure 3(a–c).

C K-edge spectra (Figure 3(a)) present a feature, fixed at 285.0 eV, assigned to C 1s(C-H) \rightarrow π^* aromatic C=C transition; the features at 287.3 eV in **1** and at 287.0 eV in **2** are assigned to C 1s \rightarrow π^* C=N/O resonance. In spectrum **1**, the features at 286.2 eV is due to C 1s(C-R) \rightarrow π^* C=C transition. In spectrum **2** the feature at 288.0 eV is associated to C 1s \rightarrow π^* C=S transition⁴⁶.

In N K-edge spectra (Figure 3(b)), the feature, fixed at 401.0 eV, is due to the 1s \rightarrow π^* transition of the C_{ar}-N bond. The previous peaks, at 400 eV in **1** and at 398.6 eV in **2**, are assigned to N 1s \rightarrow π^* C=N transition of the oxadiazole ring and to S-C=N 1s \rightarrow π^* transition⁴⁶, respectively. Finally, the two broad bands around 406 and 413 eV are assigned to N 1s \rightarrow σ^* N–H and N 1s \rightarrow σ^* N–C resonances, respectively.



Scheme 1. (i) K_2CO_3 , anhydrous DMF, 50 °C, 8 h, then r.t., 36 h. (ii) CF_3COOH , DCM, r.t., 12 h, $Et_2O \bullet HCl$, 0 °C. (iii) LiOH, NDB H_2O/THF , r.t., 12 h. (iv) NaOH 0.1 M. (v) DMF, Rhodamine-B ITC, r.t., 48 h.

Table 1. Maximum absorption wavelengths and ϵ values of NBD, Res, 1 and 2.

Sample	λ_{max} (nm)	ϵ ($cm^{-1} M^{-1}$)
NBD	469	7358
Res	310 ^a	44,307
1	325	48,574
2	280	31,401

^aAs expected from literature⁴⁵ Res absorption spectrum shows two main peaks at 310 nm and at 319 nm, respectively.

Table 2. Excitation wavelength, emission wavelength and emission intensity (a.u.) values of NBD, Res, 1 and 2.

Sample	λ_{exc} (nm)	λ_{emis} (nm)	I_{emis} (a.u.)
NBD	469	545	271
Res	325	397 ^a	53
1	458	537	19
2	319	575	271

^aEmission spectrum of Res shows one main peak at 397 nm, as expected from the literature⁴⁵.

In the O K-edge spectra (Figure 3(c)) there is a sharp peak fixed at 531.5 eV, assigned to the transition $1s \rightarrow \pi^*$ of carbonyl $C=O$. The other feature at 530.0 eV of the black spectrum is the result of the superimposition of $1s \rightarrow \pi^*$ transitions of oxadiazole oxygen and nitro group oxygens^{27,47}.

According to literature⁴⁸, in the infra-red spectrum of Ptb, features located at 1600, 1585, 1514, 1458, and 1353 cm^{-1} are mainly related to aromatic and olefinic stretching vibrations. Similar features can be detected in the spectra of samples 1 and 2 (lines b and a) (Figure 4).

The IR spectrum of 7-nitrobenzofurazan (line c) shows two main features at $1500 \times 1360 cm^{-1}$, related to asymmetric and symmetric stretching of the nitro group; the same peaks can be evidenced in the spectrum of sample 1, evidencing successful coupling of Ptb to 7-nitrobenzofurazan.

In synthesis, NEXAFS and FTIR results confirm the molecular structures proposed in Figure 1 for compounds 1 and 2.

2.3. Biocompatibility of pterostilbene derivatives

The putative cytotoxic effects of Ptb fluorescent derivatives was evaluated by the Propidium iodide (PI) assay, which is membrane impermeant and generally excluded from viable cells. This assay is commonly used for identifying dead cells in a population. In particular, the breast cancer (i.e. MCF-7) and the neuroblastoma (i.e. SH-SY5Y) cell lines have been used as experimental models and results were compared with that of Res $1 \mu M$, which shares many biosynthetic pathways with pterostilbene. Notably, none of tested

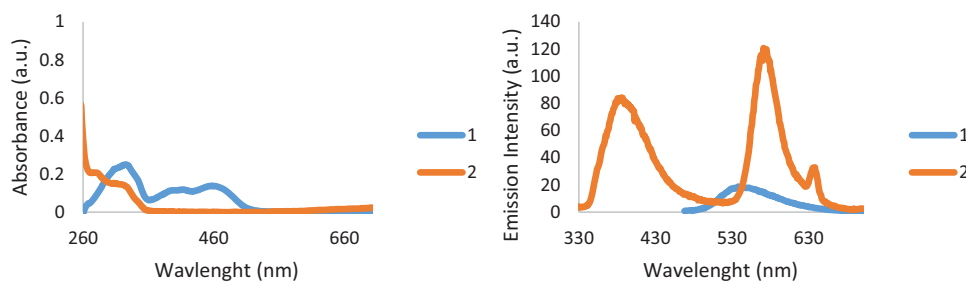


Figure 2. Absorption and emission spectra collected on 1 and 2.

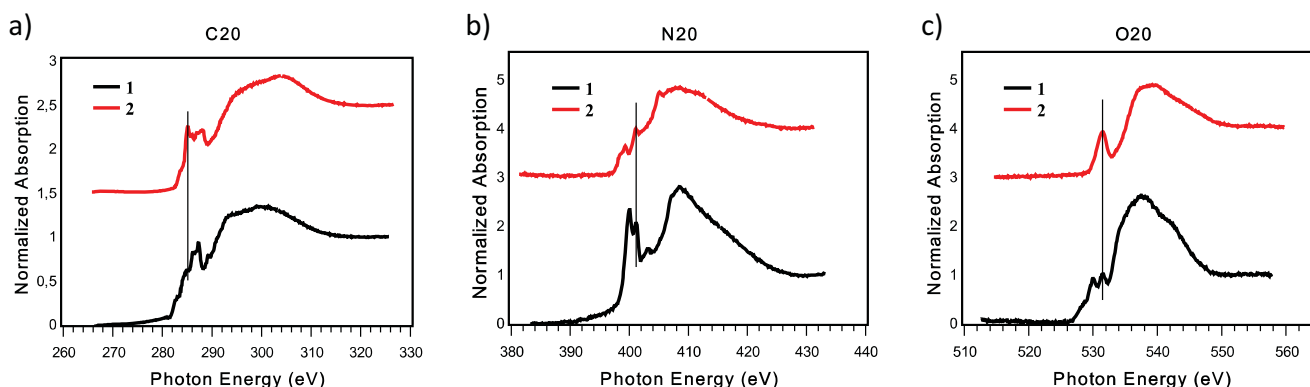


Figure 3. Carbon K-edge spectrum (a), nitrogen K-edge spectrum (b), and oxygens K-edge spectrum (c) of samples 1 and 2.

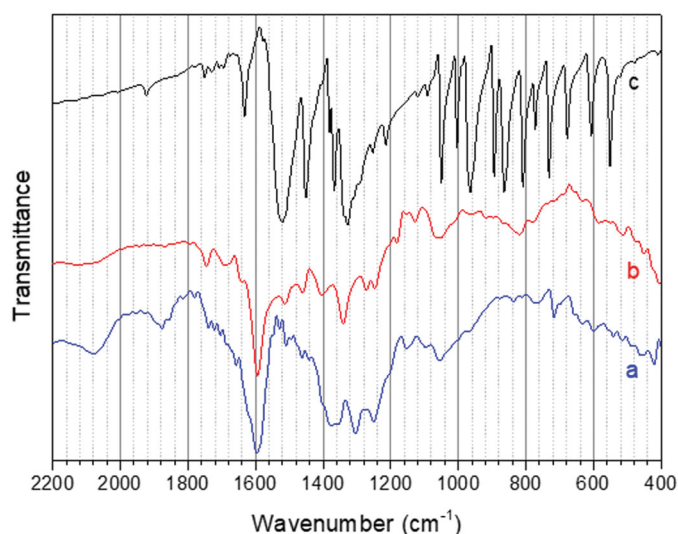


Figure 4. FTIR spectra of samples 2 (a), 1 (b) and of 7-nitrobenzofurazan (c).

concentrations (i.e. 0.1–10.0 μM) of Ptb or its fluorescent derivatives modified cell morphology (data not shown) or their vitality (Figure 5(a)). The compounds effects on cell vitality were further confirmed evaluating the activation of poly (ADP-ribose) polymerase-1 (PARP-1) cleavage (Figure 5(b)). PARP-1, a DNA-binding enzyme involved in DNA repair, is a hallmark of the process of programmed cell death or apoptosis⁴⁹. Neither Ptb nor its derivatives (1, 2) modify cell vitality or promote PARP-1 cleavage confirming the very low toxicity of this compound as already reported^{29,33}. Of note, none of Ptb derivatives reduces the cell number nor activates the apoptotic cascade, sustaining the inability of these compounds to trigger a stress-dependent signal transduction pathway.

The lack of any toxic effects of Ptb fluorescent derivatives (1, 2) raised the question if these compounds still maintain some of

neuro-protective effects ascribed to their precursor^{50,51}. The discovery that high levels of neuroglobin (NGB), an endogenous neuroprotective globin, are active against several brain injuries, including neurodegeneration, hypoxia, ischaemia, toxicity, and nutrient deprivation prompted us to evaluate the effect of different concentrations of Ptb and their fluorescent derivatives in SH-SY5Y cells. Res 1 μM , which increased NGB levels in neuronal derived cells reducing globin levels in breast cancer cells⁵², was used as positive control. As expected, Res increased NGB levels by 58% \pm 0.6, Ptb 10 μM shows the same efficacy than Res (1 μM) although it is less effective increasing NGB levels by 30% \pm 0.4. The compound 1 maintained the same efficacy than Res, with a value higher with respect to its precursor (Ptb), whereas the compound 2 reduced NGB levels under the control value. As a whole, these data, for the first time, indicate that Ptb neuroprotective effects, like Res, could be mediated by the accumulation of NGB suggesting that both polyphenols could share the same signalling pathways. Moreover, only Ptb functionalised on phenolic ring with benzofurazan (compound 1) maintained the same efficacy of its precursor in enhancing NGB levels, while Ptb derivative containing rhodamine B-isothiocyanate (compound 2) significantly reduced NGB levels under the control values, Figure 6.

Nowadays, NGB is regarded as an endogenous neuroprotective haeme-protein being active against several brain injuries, including hypoxia, ischaemia, toxicity, and O₂/nutrient deprivation. The correlation between NGB expression and protection against nervous system pathologies has been demonstrated in cell systems, *in vivo* models of ND, and in human beings. Aside from the nature of the insult considered, NGB protective effects seem to depend on its overexpression and mitochondrial localisation⁵³. Thus, it is not surprising that research in the field of neurodegeneration focuses on NGB inducers¹⁴. Among different NGB inducers, 17 β -oestradiol (E2) deserves a particular attention as physiological concentrations of this hormone induce a 300% increase of NGB levels in human SKN-BE neuroblastoma cell line, mouse hippocampal neurons, primary cortical astrocytes, and striatal neurons via

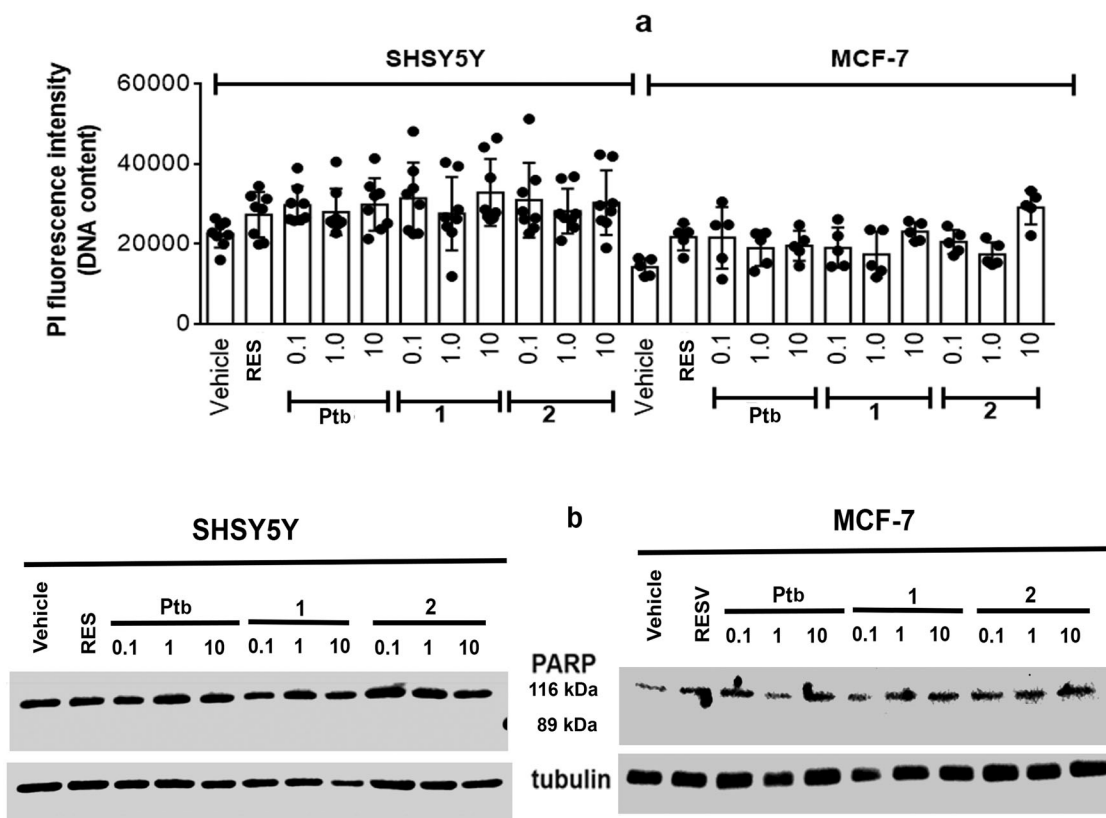


Figure 5. Analyses of cellular DNA content obtained from propidium iodide assay (PI) in SH-SY5Y neuroblastoma (left) and MCF-7 breast cancer (right) cells. (a) Cells were treated for 48 h with either vehicle (ethanol/DMEM, 1/10) or resveratrol (Res, 1 μ M) or with different Pterostilbene (Ptb) or its fluorescent derivatives (1 and 2) concentrations. Data are means \pm SD of height (SH-SY5Y) or five (MCF-7) different experiments. (b) Typical Western blot of five different experiments of PARP-1 (uncleaved 116 kDa, cleaved 89 kDa) in cells treated as in (a).

oestrogen receptor (ER) β -activated rapid and transcriptional events. Moreover, ligands of the subtype β of oestrogen receptor (ER β) (e.g. Res and Ptb⁵⁴) enhance the endogenous NGB levels facilitating neuron resilience to the stress⁵². Our data sustain that, like Res, Ptb, and its benzofurazan derivative (compound 1, see Figure 1) could activate the ER β pathway in SH-SY5Y neurons, while the Ptb derivative containing rhodamine B-isothiocyanate (compound 2, see Figure 1) seems to be unable to activate the ER β . The different biological profiles between 1 and 2 might be attributed to the great steric hindrance of rhodamine B-isothiocyanate moiety that could inhibit or impede the binding of 2 to this oestrogen receptor subtype. On the other hand, the SH-SY5Y cells, as other cells of neuronal origin, also express less levels of ER α ⁵², the other oestrogen receptor subtype, which inhibition could explain the decrease of NGB levels. These data will be confirmed experimentally in the next future and our laboratory is currently very active on these issues.

The results obtained in this study highlight compound 1 as a good candidate for future studies as neuroprotective compound endowed of a good biocompatibility, absence of cellular toxicity, and the ability to be a NGB inducer as resveratrol.

3. Experimental section

3.1. Chemistry

Reagents and solvents of analytical grade were purchased from Sigma-Aldrich (St. Louis, MO) and from Fluorochem (Hadfield, UK), and were used without further purification. Chemical reactions were monitored by thin layer chromatography (TLC) using aluminium plates pre-coated with silica gel and containing a fluorescent

indicator (Merck Silica Gel 60 F254). The spots on TLC were visualised by a UV lamp (254 nm). Na₂SO₄ was used as dehydrating agents for solutions, while they were evaporated *in vacuo* with a rotating evaporator.

Flash chromatographic purifications were performed in glass columns using silica gel 230–400 mesh Sigma-Aldrich (St. Louis, MO). Compounds were characterised by the determination of melting points and of NMR and Mass Spectrometry spectra. Melting points (m.p.) were measured with a *Leica Galen III* microscope. ¹H and ¹³C NMR spectra were recorded in the opportune solvent with a Bruker Ultrashield™ 400 MHz spectrometer (Fallander, Switzerland), at 25 °C. Chemical shifts (δ) are given in ppm and coupling constants (*J*) are reported in Hz. Signals in NMR spectra are indicated by the following abbreviations: *s* = singlet, *d* = doublet, *t* = triplet, *q* = quartette, *m* = multiplet, *bs* = broad singlet. Mass spectra (ESI-MS) were recorded with a high-resolution Q Exactive plus Orbitrap spectrometer (Thermo Fisher Scientific, Waltham, MA), resolution 140,000 at *m/z* 200.

3.1.1. Synthesis of (E)-tert-butyl (2-(4-(3,5-dimethoxystyryl)phenoxy)ethyl)carbamate (5)

To a solution of 4-(3,5-dimethoxystyryl)phenol 3 (0.91 mmol, 1 Eq.) and K₂CO₃ (1.82 mmol, 2 Eq.) in anhydrous DMF (2 ml) and was added dropwise, under nitrogen, a solution of N-Boc-ethylamine bromide 4 (0.91 mmol, 1 Eq.) in anhydrous DMF. The reaction mixture was stirred at 50 °C for 8 h and then left to r.t. for 36 h monitoring by TLC. Then H₂O was added and the aqueous solution was extracted with CHCl₃. The organic phase was washed twice with H₂O and ice, dehydrated with Na₂SO₄ and finally evaporated

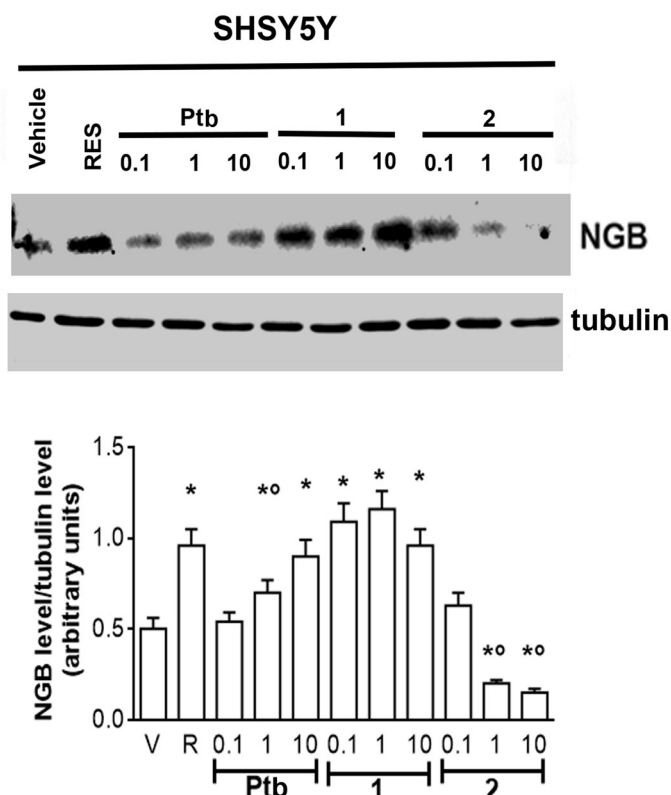


Figure 6. Effect of pterostilbene (Ptb) and its fluorescent derivatives (1 and 2) on neuroglobin (NGB) levels in neuronal-derived cells. Western blot (upper panel) and densitometric analyses (bottom panel) of NGB levels in SH-SY5Y cells. Cells were treated for 24 h with resveratrol (R, 1 μ M) or with different compound concentrations. The amount of NGB was normalised by comparison with α -tubulin levels. Data are the mean \pm SD of five different experiments. $p < 0.001$ was determined with ANOVA followed by Bonferroni test with respect to the vehicle (*) or to R-treated samples (*o).

under reduced pressure in rotating evaporator. Compound **5** was obtained as a transparent oil (95% yield). $^1\text{H NMR}$ (400 MHz, CDCl_3) δ : 8.01 (s, 1H, NH); 7.44–7.41 (d, 2H, $J = 8.7$ Hz, Ar); 7.04–7.00 (d, 1H, $J = 16.2$ Hz, CH=CH); 6.91–6.87 (d, 1H, $J = 16.2$ Hz, CH=CH); 6.89–6.83 (m, 2H, Ar); 6.64–6.63 (d, 2H, $J = 2.2$ Hz, Ar); 6.37–6.36 (t, 1H, $J = 2.2$ Hz, Ar); 4.04–4.01 (t, 2H, $J = 5.0$ Hz, CH_2); 3.82 (s, 6H, OCH_3); 3.54–3.52 (t, 2H, $J = 5.0$ Hz, CH_2); 1.45 (s, 9H, t-Bu).

3.1.2. Synthesis of (E)-(4-(3,5-dimethoxystyryl)phenoxy)methanamine hydrochloride (6)

To a solution of compound **5** (0.82 mmol, 1 Eq.) in DCM (10 ml), was added dropwise TFA (5.74 mmol, 7 Eq.). The reaction mixture was left stirring overnight at r.t. The reaction mixture was then neutralised with saturated solution of NaHCO_3 to pH \sim 8. The aqueous solution was extracted with DCM and the organic phase was washed twice with H_2O . The organic phase was dried with Na_2SO_4 and evaporated under reduced pressure. To the pale-yellow oil obtained was added a solution of $\text{Et}_2\text{O} \bullet \text{HCl}$, dropwise at 0°C , to get the hydrochloride salt and then solution was evaporated. The crude product was purified by trituration in Et_2O to afford compound **6** as a pink solid (61% yield). $^1\text{H NMR}$ (400 MHz, $\text{CD}_3\text{OD}-d_4$) δ : 7.04–7.02 (d, 2H, $J = 8.7$ Hz, Ar); 6.64–6.59 (d, 1H, $J = 16.3$ Hz, CH=CH); 6.53–6.51 (d, 2H, $J = 8.7$ Hz, Ar); 6.51–6.47 (d, 1H, $J = 16.3$ Hz, CH=CH); 6.20–6.19 (d, 2H, $J = 2.2$ Hz, Ar); 5.89–5.88 (t, 1H, $J = 2.2$ Hz, Ar); 3.77–3.74 (t, 2H, $J = 5.0$ Hz, CH_2); 3.31 (s, 6H, OCH_3); 2.89–2.87 (t, 2H, $J = 5.0$ Hz, CH_2).

3.1.3. Synthesis of (E)-N-(2-(4-(3,5-dimethoxystyryl)phenoxy)ethyl)-7-nitrobenzo[c][1,2,5]oxadiazol-4-amine (1)

Compound **6** (0.60 mmol, 1 Eq.) and commercially available 4-chloro-7-nitrobenzofurazan **7** (0.60 mmol, 1 Eq.) were dissolved in a $\text{H}_2\text{O}/\text{THF}$ solution. To the resulting solution was added LiOH (0.66 mmol, 1.1 Eq.) and then the mixture was stirred at r.t. overnight, protected from light. The brown solid precipitate was washed with H_2O and filtered under vacuum. The crude product was purified by flash chromatography (n -hexane/ EtOAc in ratio 1.5:1) and then triturated in n -hexane. Compound **1** was obtained as a brown solid (93% yield). M.p.: $166\text{--}168^\circ\text{C}$. $^1\text{H NMR}$ (400 MHz, $\text{DMSO}-d_6$) δ : 9.61 (s, 1H, NH); 8.56–8.54 (d, 1H, $J = 8.7$ Hz, Ar); 7.53–7.51 (d, 2H, $J = 8.7$ Hz, Ar); 7.22–7.18 (d, 1H, $J = 16.4$ Hz, CH=CH); 7.03–6.99 (d, 1H, $J = 16.4$ Hz, CH=CH); 6.97–6.95 (d, 2H, $J = 8.7$ Hz, Ar); 6.73–6.72 (d, 2H, $J = 2.0$ Hz, Ar); 6.58–6.55 (d, 1H, $J = 8.7$ Hz, Ar); 6.38–6.37 (d, 1H, $J = 2.0$ Hz, Ar); 4.33–4.31 (t, 2H, OCH_2); 3.90 (bs, 2H, $\text{CH}_2\text{-NH}$); 3.76 (s, 6H, OCH_3). $^{13}\text{C NMR}$ (100 MHz, $\text{DMSO}-d_6$) δ : 159.8 (2C, Ar- OCH_3); 157.9 (1C, Ar); 145.3, 144.4 (2C, C=N); 139.3; 137.9 (2C, Ar); 129.9 (2C, CH=CH); 128.4, 127.8 (3C, Ar); 126.3 (1C, Ar- NO_2); 121.1; 114.7; 104.1; 99.7 (7C, Ar); 65.4 (1C, CH_2); 55.1 (2C, OCH_3); 43.0 (1C, CH_2). m/z ESI-MS: $[\text{M}-\text{H}]^-$ 461.15.

3.1.4. Synthesis of (E)-2-(3,6-bis(diethylamino)-4aH-xanthen-9-yl)-5-(3-(2-(4-(3,5-dimethoxystyryl)phenoxy)ethyl)thioureido)benzoic acid (2)

Compound **6** (0.19 mmol, 1 Eq.), as hydrochloride salt, was precipitated in 10 ml of NaOH 0.1 M. The resulting precipitate was solubilised in 5 ml of DMF, and then Rhd B-Itc **8** (0.19 mmol, 1 Eq.) was added to the solution. The reaction mixture was left stirring 48 h at r.t. and protected from light. The reaction was monitored by TLC. The aqueous solution was extracted with EtOAc and then the organic layer was washed with H_2O . The organic phase was dried over Na_2SO_4 and concentrated *in vacuo*. The crude product was purified by flash chromatography ($\text{CH}_2\text{Cl}_2/\text{MeOH}$, 9.5:0.5 \rightarrow 9:1) to afford compound **2** as a red solid (12% yield). M.p. $140\text{--}142^\circ\text{C}$. $^1\text{H NMR}$ (400 MHz, $\text{CD}_3\text{OD}-d_4$) δ : 7.96 (s, 1H, Ar); 7.82–7.80 (m, 1H, Ar); 7.46–7.44 (d, 2H, $J = 8.6$ Hz, Ar); 7.36–7.33 (d, 2H, $J = 9.5$ Hz, Ar); 7.18–7.16 (d, 1H, $J = 8.6$ Hz, Ar); 7.07–7.03 (d, 1H, $J = 16.2$ Hz, CH=CH); 6.99–6.88 (m, 5H, Ar); 6.98–6.95 (d, 2H, $J = 9.5$ Hz, Ar); 6.92–6.88 (d, 1H, $J = 16.2$ Hz, CH=CH); 6.64–6.63 (d, 2H, $J = 2.2$ Hz, Ar); 6.36–6.35 (t, 1H, $J = 2.2$ Hz, Ar); 4.28–4.25 (t, 2H, $J = 5.4$ Hz, CH_2); 4.06–4.03 (t, 2H, $J = 5.4$ Hz, CH_2); 3.79 (s, 6H, OCH_3); 3.66–3.61 (q, 8H, CH_2); 1.30–1.26 (m, 12H, CH_3). $^{13}\text{C NMR}$ (100 MHz, $\text{MeOD}-d_4$) δ : 183.0 (1C, C=S); 163.4 (1C, COOH); 162.7 (2C, Ar- OCH_3); 160.2 (1C, Ar- OCH_2); 159.6, 157.0, 141.3, 133.5, 132.0, 131.4, 130.0 (11C, Ar); 129.1 (2C, CH=CH); 128.0, 116.2, 115.4, 115.0, 105.5, 100.7, 97.2 (17C, Ar); 67.5 (1C, OCH_2); 56.0 (2C, OCH_3); 46.9 (4C, CH_2); 45.4 (1C, CH_2); 33.3, 30.9, 23.9; 14.6, 13.0 (4C, CH_3). m/z ESI-MS: $[\text{M} + \text{H}]^+$ 799.35.

3.2. Optical and structural characterisations

UV-visible absorption measurements were carried out in the range 200–800 nm, using DMSO solution in quartz cells, by Shimadzu 2401 PC UV-vis spectrophotometer⁵⁵. Fluorescence measurements were carried out, using DMSO solution in quartz cells, by Varian-Carey Eclipse Fluorescence Spectrophotometer.

Fourier transform infra-red spectroscopy (FT-IR) spectra have been recorded in the $4000\text{--}400\text{ cm}^{-1}$ range with a Bruker Vector 22 equipped with a DTGS detector. Thin films of samples **1** and **2**, deposited from DMSO solution onto gold substrates, were

analysed in reflectance mode with a Specac P/N 19650 series monolayer/grazing angle accessory. KBr pellets of 7-nitrobenzofurazan samples were prepared to record the FTIR spectrum.

Near-edge X-ray absorption fine structure (NEXAFS) spectra were acquired at the BEAR beamline (bending magnet for emission absorption and reflectivity) at the ELETTRA storage ring. BEAR is installed at the left exit of the 8.1 bending magnet exit. The apparatus is based on a bending magnet as a source and beam-line optics delivering photons from 5 eV up to about 1600 eV with selectable degree of ellipticity. The UHV end station is equipped with a movable hemispherical electron analyser and a set of photodiodes to collect angle-resolved photoemission spectra, optical reflectivity, and fluorescence yield. In these experiments, we used ammeters to measure drain current from the sample. C, N, and O K-edge spectra were collected at grazing (20°) incidence angles of the linearly polarised photon beam with respect to the sample surface. In addition, our carbon, nitrogen and oxygen K-edge spectra have been further calibrated using the resonance at 285.00 eV, assigned to the C=C aromatic $1s - \pi^*$ transition, the resonance at 401.00 eV, assigned to the $1s - \pi^*$ transition of the C_{ar}-N bond and the resonance at 531.5 eV, assigned to the C=O carbonyl $1s - \pi^*$ transition, respectively. The raw C, N, and O K-edge NEXAFS spectra were normalised to the incident photon flux by dividing the sample spectrum by the spectrum collected on a freshly sputtered gold surface. Spectra were then normalised subtracting a straight line that fits the part of the spectrum below the edge and assessing to 1 the value at 330.00, 430.00, and 560.00 eV for carbon, nitrogen, and oxygen, respectively.

3.3. Cell lines and in vitro assays

3.3.1. Cell culture and stimulation

Human breast cancer cells, MCF-7, and human neuroblastoma cells, SH-SY5Y (ATTC, LGC Standards S.r.l., Milano, Italy) were grown in air containing 5% CO₂ in modified, phenol red-free, Dulbecco's Modified Eagle's Medium (DMEM) medium. Ten % (vol/vol) of charcoal-stripped foetal calf serum, L-glutamine (2 mM), gentamicin (0.1 mg/mL), and penicillin (100 U/mL) were added to the media before use. Cells were used at passage 13–17. The cell line authentication was periodically performed by amplification of multiple short tandem repeat loci by BMR genomics S.r.l (Padova, Italy). Cells were treated for 48 h with either vehicle (ethanol [EtOH]/DMEM, 1:10; vol/vol) or resveratrol (Res, 1 μM) or with different concentration of Pterostilbene and its fluorescent derivatives **1** and **2**.

3.3.2. Western blot assay

Briefly, after the treatments, cells were lysed and protein were solubilised in the YY buffer (50 mM HEPES at pH 7.5, 10% glycerol, 150 mM NaCl, 1% Triton X-100, 1 mM EDTA, and 1 mM EGTA) containing 0.70% (wt/vol) sodium dodecyl sulphate (SDS). Total proteins were quantified using the Bradford protein assay (Bio-Rad Laboratories, Hercules, CA). Solubilised proteins (20 μg) were resolved by 7% or 15% SDS-polyacrylamide gel electrophoresis at 100 V for 1 h at 24.0 °C and then transferred to nitrocellulose with the Trans-Blot Turbo Transfer System (Bio-Rad Laboratories, Hercules, CA) for 10 min. The nitrocellulose was treated with 5% (wt/vol) bovine serum albumin in 138.0 mM NaCl, 25.0 mM Tris, pH 8.0, at 24.0 °C for 1 h and then probed overnight at 4.0 °C with anti-PARP-1 (final dilution, 1:1000) or with anti-NGB (final dilution, 1:1000) antibodies. Moreover, anti- α -tubulin (final dilution, 1:30,000) antibody was used to normalise the protein loaded. The

antibody reaction was visualised with the chemiluminescence western blot analysis detection reagent (Amersham Biosciences, Little Chalfont, UK). The densitometric analyses were performed by the ImageJ software for Microsoft Windows (National Institute of Health, Bethesda, MD).

3.3.3. Propidium iodide (PI) assay

After grown up to 80% confluence in 96-well plate, cells were stimulated as reported above. Fixation and permeabilization were performed through ice cold EtOH 70% for 15 min at −20 °C. After EtOH solution removal, the cells were incubated with PI buffer for 30 min in the dark. Again, solution removal was performed, and the cells were rinsed with PBS solution. The fluorescence was revealed (excitation wavelength: 537 nm; emission wavelength: 621 nm) with TECAN Spark 20M multimode microplate reader (Life Science, Padua, Italy).

3.3.4. Statistical analysis

The statistical analyses were performed by Student's *t*-test to compare two sets of data or by ANOVA followed by Bonferroni test to compare different group of data by INSTAT software system for Windows. In all cases, $p < 0.05$ was considered significant.

Disclosure statement

No potential conflict of interest was reported by the authors.

Funding

This research was supported by the PRIN 2017 grant prot. 20175NRXH3 from the Italian Ministry of Education, University and Research (MIUR).

ORCID

Lidia Ciccone  <http://orcid.org/0000-0002-2762-1929>

References

1. Alzheimer's Disease International. World Alzheimer Report 2019 [Internet]. Available from: <https://www.alz.co.uk/research/WorldAlzheimerReport2019.pdf>.
2. 2021 Alzheimer's Disease Facts and Figures. Alzheimer's Dement 2021;17:327–406.
3. Breijyeh Z, Karaman R. Comprehensive review on Alzheimer's disease: causes and treatment. Molecules 2020; 25:5789.
4. Raza C, Anjum R, Shakeel NA. Parkinson's disease: mechanisms, translational models and management strategies. Life Sci 2019;226:77–90.
5. Cappella M, Ciotti C, Cohen-Tannoudji M, Biferi MG. Gene therapy for ALS—a perspective. Int J Mol Sci 2019;20:4388.
6. Ricci F, Bandello F, Navarra P, et al. Neovascular age-related macular degeneration: therapeutic management and new-upcoming approaches. Int J Mol Sci 2020;21:8242.
7. Canady VA. FDA approves first drug therapy for Alzheimer's in 18 years. Mental Health Weekly 2021;31:3–4.
8. Walsh S, Merrick R, Milne R, Brayne C. Aducanumab for Alzheimer's disease? BMJ 2021;374:n1682.

9. Aducanumab. *EMBO Mol Med* 2021;13:e14781.
10. Andrade S, Ramalho MJ, Loureiro JA. Natural compounds for Alzheimer's disease therapy: a systematic review of preclinical and clinical studies. *Int J Mol Sci* 2019;41:2313.
11. Ciccone L, Tonali N, Nencetti S, Orlandini E. Natural compounds as inhibitors of transthyretin amyloidosis and neuroprotective agents: analysis of structural data for future drug design. *J Enzyme Inhib Med Chem* 2020;35:1145–62.
12. Bernardini S. Natural products for human health: an historical overview of the drug discovery approaches. *Nat Prod Res* 2017;26:1–25.
13. Ciccone L, Vandoooren J, Nencetti S, Orlandini E. Natural marine and terrestrial compounds as modulators of matrix metalloproteinases-2 (MMP-2) and MMP-9 in Alzheimer's disease. *Pharmaceutics* 2021;14:86.
14. Ciccone L, Nencetti S, Socci S, Orlandini E. Neuroglobin and neuroprotection: the role of natural and synthetic compounds in neuroglobin pharmacological induction. *Neural Regen Res* 2021;16:2353–8.
15. Carresi C, Scicchitano M, Scarano F, et al. The potential properties of natural compounds in cardiac stem cell activation: their role in myocardial regeneration. *Nutrients* 2021;13:275.
16. Li W, Sun K, Hu F, et al. Protective effects of natural compounds against oxidative stress in ischemic diseases and cancers via activating the Nrf2 signaling pathway: a mini review. *J Biochem Mol Toxicol* 2021;35:e22658.
17. Kamal M, Naz M, Jawaid T, Arif M. Natural products and their active principles used in the treatment of neurodegenerative diseases: a review. *Orient Pharm Exp Med* 2019;19:343–65.
18. Weller J, Budson A. Current understanding of Alzheimer's disease diagnosis and treatment. *F1000Res* 2018;7:1161.
19. Ahmed T, Javed S, Javed S, et al. Resveratrol and Alzheimer's disease: mechanistic insights. *Mol Neurobiol* 2017;54:2622–35.
20. Xia D, Sui R, Zhang Z. Administration of resveratrol improved Parkinson's disease-like phenotype by suppressing apoptosis of neurons via modulating the MALAT1/miR-129/SNCA signaling pathway. *J Cell Biochem* 2019;120:4942–51.
21. Chen J-Y, Zhu Q, Zhang S, et al. Resveratrol in experimental Alzheimer's disease models: a systematic review of preclinical studies. *Pharmacol Res* 2019;150:104476.
22. Arbo BD, André-Miral C, Nasre-Nasser RG, et al. Resveratrol derivatives as potential treatments for Alzheimer's and Parkinson's disease. *Front Aging Neurosci* 2020;12:103.
23. Wang D, Ho L, Faith J, et al. Role of intestinal microbiota in the generation of polyphenol-derived phenolic acid mediated attenuation of Alzheimer's disease β -amyloid oligomerization. *Mol Nutr Food Res* 2015;59:1025–40.
24. Moussa C, Hebron M, Huang X, et al. Resveratrol regulates neuro-inflammation and induces adaptive immunity in Alzheimer's disease. *J Neuroinflammation* 2017;14:1.
25. Fang X, Zhang J, Zhao J, Wang L. Effect of resveratrol combined with donepezil hydrochloride on inflammatory factor level and cognitive function level of patients with Alzheimer's disease. *J Healthc Eng* 2022;2022:e9148650–e9148657.
26. Turner RS, Thomas RG, Craft S, Study F the ADC, et al. A randomized, double-blind, placebo-controlled trial of resveratrol for Alzheimer disease. *Neurology* 2015;85:1383–91.
27. Venditti I, Lucci G, Fratoddi I, et al. Direct conjugation of resveratrol on hydrophilic gold nanoparticles: structural and cytotoxic studies for biomedical applications. *Nanomaterials* 2020;10:1898.
28. Poulouse SM, Thangthaeng N, Miller MG, Shukitt-Hale B. Effects of pterostilbene and resveratrol on brain and behavior. *Neurochem Int* 2015;89:227–33.
29. Estrela JM, Ortega A, Mena S, et al. Pterostilbene: biomedical applications. *Crit Rev Clin Lab Sci* 2013;50:65–78.
30. Kapetanovic IM, Muzzio M, Huang Z, et al. Pharmacokinetics, oral bioavailability, and metabolic profile of resveratrol and its dimethylether analog, pterostilbene, in rats. *Cancer Chemother Pharmacol* 2011;68:593–601.
31. Kim H, Seo K-H, Yokoyama W. Chemistry of pterostilbene and its metabolic effects. *J Agric Food Chem* 2020;68:12836–41.
32. Wang P, Sang S. Metabolism and pharmacokinetics of resveratrol and pterostilbene. *BioFactors* 2018;44:16–25.
33. Riche DM, McEwen CL, Riche KD, et al. Analysis of safety from a human clinical trial with pterostilbene. *J Toxicol* 2013;2013:e463595.
34. Lange KW, Li S. Resveratrol, pterostilbene, and dementia. *BioFactors* 2018;44:83–90.
35. Deng L, Li Y, Zhang X, et al. UPLC–MS method for quantification of pterostilbene and its application to comparative study of bioavailability and tissue distribution in normal and Lewis lung carcinoma bearing mice. *J Pharm Biomed Anal* 2015;114:200–7.
36. Liu Y, You Y, Lu J, et al. Recent advances in synthesis, bioactivity, and pharmacokinetics of pterostilbene, an important analog of resveratrol. *Molecules* 2020;25:5166.
37. Cherniack EP. A berry thought-provoking idea: the potential role of plant polyphenols in the treatment of age-related cognitive disorders. *Br J Nutr* 2012;108:794–800.
38. Chang J, Rimando A, Pallas M, et al. Low-dose pterostilbene, but not resveratrol, is a potent neuromodulator in aging and Alzheimer's disease. *Neurobiol Aging* 2012;33:2062–71.
39. Liu H, Wu X, Luo J, et al. Pterostilbene attenuates astrocytic inflammation and neuronal oxidative injury after ischemia-reperfusion by inhibiting NF- κ B phosphorylation. *Front Immunol* 2019;10:2408.
40. Song Z, Han S, Pan X, et al. Pterostilbene mediates neuroprotection against oxidative toxicity via oestrogen receptor α signalling pathways. *J Pharm Pharmacol* 2015;67:720–30.
41. Yanagi M, Uchida N, Hamada H. Versatile synthetic route for resveratrol modification via amine functionalization. *Nat Prod Commun* 2019;14:1934578X1987621.
42. Komatsu S, Ohno K, Fujimura T. Binding assays using a benzofurazan-labeled fluorescent probe for estrogen receptor–ligand interactions. *Chem Pharm Bull* 2020;68:954–61.
43. Uchiyama S, Santa T, Okiyama N, et al. Fluorogenic and fluorescent labeling reagents with a benzofurazan skeleton. *Biomed Chromatogr* 2001;15:295–318.
44. Beiija M, Afonso CAM, Martinho JMG. Synthesis and applications of Rhodamine derivatives as fluorescent probes. *Chem Soc Rev* 2009;38:2410–33.
45. Zhang J, Mi Q, Shen M. Resveratrol binding to collagen and its biological implication. *Food Chem* 2012;131:879–84.
46. Graf N, Lippitz A, Gross T, et al. Determination of accessible amino groups on surfaces by chemical derivatization with 3,5-bis(trifluoromethyl)phenyl isothiocyanate and XPS/NEXAFS analysis. *Anal Bioanal Chem* 2010;396:725–38.
47. Giebler R, Schulz B, Reiche J, et al. Near-edge X-ray absorption fine structure spectroscopy on ordered films of an

- amphiphilic derivate of 2,5-diphenyl-1,3,4-oxadiazole. *Langmuir* 1999;15:1291–8.
48. Liu Q, Chen J, Qin Y, et al. Zein/fucoidan-based composite nanoparticles for the encapsulation of pterostilbene: preparation, characterization, physicochemical stability, and formation mechanism. *Int J Biol Macromol* 2020;158:461–70.
 49. Chaitanya GV, Steven AJ, Babu PP. PARP-1 cleavage fragments: signatures of cell-death proteases in neurodegeneration. *Cell Commun Signal* 2010;8:31.
 50. Yan W, Ren D, Feng X, et al. Neuroprotective and anti-inflammatory effect of pterostilbene against cerebral ischemia/reperfusion injury via suppression of COX-2. *Front Pharmacol.* 2021;12:770329.
 51. Zhou Y, Zhang X, Ma A, et al. Orally administrated pterostilbene attenuates acute cerebral ischemia–reperfusion injury in a dose- and time-dependent manner in mice. *Pharmacol Biochem Behav* 2015;135:199–209.
 52. Cipolletti M, Montalesi E, Nuzzo MT, et al. Potentiation of paclitaxel effect by resveratrol in human breast cancer cells by counteracting the 17β -estradiol/estrogen receptor α /neuroglobin pathway: CIPOLLETTI ET AL. *J Cell Physiol* 2019;234:3147–57.
 53. Fiocchetti M, Cracco P, Montalesi E, et al. Neuroglobin and mitochondria: the impact on neurodegenerative diseases. *Arch Biochem Biophys* 2021;701:108823.
 54. Robb EL, Stuart JA. The stilbenes resveratrol, pterostilbene and piceid affect growth and stress resistance in mammalian cells via a mechanism requiring estrogen receptor beta and the induction of Mn-superoxide dismutase. *Phytochemistry* 2014;98:164–73.
 55. Fratoddi I, Venditti I, Battocchio C, et al. Highly hydrophilic gold nanoparticles as carrier for anticancer copper(I) complexes: loading and release studies for biomedical applications. *Nanomaterials* 2019;9:772.